Eur. Phys. J. D **21**, 167–179 (2002)
DOI: 10.1140/epjd/e2002-00194-y

THE EUROPEAN PHYSICAL JOURNAL D

The use of high energy laser-plasma sources in soft X-ray contact microscopy of living biological samples

D. Batani[1,a], C. Botto[1], M. Moret[1], M. Milani[1], G. Lucchini[1], K. Eidmann[2], F. Cotelli[3], C. Lora Lamia Donin[3], G. Poletti[3], T. Ford[4], and A. Stead[4]

[1] Università degli Studi di Milano-Bicocca and INFM, Piazza della Scienza 3, 20126 Milano, Italy
[2] Max Planck Institut für Quantenoptik, Garching, Germany
[3] Università di Milano, 20126 Milano, Italy
[4] Royal Holloway, University of London, London, UK

Received 5 June 2002
Published online 24 September 2002 –

Abstract. In this paper the results of an experiment on soft X-ray contact microscopy using a laser-plasma source are presented. A resolution of 50 nm has been achieved imaging pig sperm cells, while other specimens, such as algae and yeast cells, showed internal details, proving the technique to be a powerful tool for biological investigations. Original biological information has been obtained and the conditions for optimal image formation have been studied.

PACS. 07.85.-m X- and gamma-ray instruments – 52.50.Jm Plasma production and heating by laser beams (laser-foil, laser-cluster, etc.) – 78.70.En X-ray emission spectra and fluorescence

1 Introduction

Soft X-ray Contact Microscopy (SXCM) is a technique devised to produce images of biological samples with a resolution higher than optical microscopy, using a shorter wavelength radiation. With respect to other imaging techniques, such as Electron Microscopy (EM), it avoids the drawbacks due to sample preparation: in EM, in fact, the specimens must be fixed, dehydrated, embedded in resin, cut in thin sections and stained with heavy metals. Potentially any of these processes may introduce artefacts [1], and thus the possibility of studying living samples is precluded. SXCM allows living cells to be imaged, leaving them in a liquid environment [2,3]. An additional advantage is the easier handling of the samples. These advantages are due to the existence of a particular region of the electromagnetic spectrum, called the Water Window (WW), which lies between the absorption edges of carbon (280 eV) and of oxygen (530 eV). In the WW region, water is almost transparent to X-rays, while carbon, which is the main constituent of cell structures, is highly opaque, therefore it is possible to produce high contrast images of organic samples.

Laser plasmas seem to be an ideal X-ray source [4]: the hot and dense plasma produced in the interaction of a laser pulse with a solid target [5] can yield high fluxes of radiation, whose spectrum can be chosen by changing the target material and beam focusing. The short irradiation time, of the order of the laser pulse, is far below the time needed by radiation to damage the sample (of the order of ms), therefore producing images of the cell when it is still alive [6,7], and not influenced by radiation damage nor affected by movement of either the specimen or the structures within the cell.

The images are obtained by exposing the samples as a 1:1 radiograph on a photo resist, which is then chemically developed and finally analysed using an Atomic Force Microscope (AFM) [8]. In this way no optics are required. This is significant because in the soft X-ray region optics are still expensive and not very efficient.

Although SXCM is not a completely new technique, it still remains largely qualitative, and the problem of reproducibility remains. In fact the actual conditions of biological samples and X-ray emission have been almost never fully characterised in SXCM experiments.

Currently part of the research in SXCM is focusing on the development of table top systems which could allow images to be directly obtained in biological laboratories [9]. Nevertheless we think that only by using high energy lasers is it possible to understand how the image quality can be improved, *i.e.* how to obtain high resolution and better contrast, and how the problems of characterisation and reproducibility can be solved. Indeed high energy sources enable the characterisation of every laser shot through the use of different diagnostics and to obtain many images per shot, whose quality can then be correlated with the source parameters. Furthermore, with small laser systems, only high Z targets, having high laser to X-ray conversion efficiencies, can be used, allowing images to be recorded in a single shot [10,11]. Instead high

[a] e-mail: batani@mib.infn.it

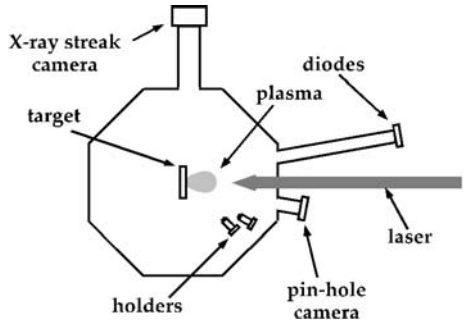

Fig. 1. Experimental set-up.

energy laser pulses permit the use of different targets with convenient X-ray spectra even if they have a lower conversion efficiency [12,13]. This is important because such sources may have a "cleaner" spectrum, *i.e.* less X-rays outside the WW.

For all these reasons we performed an experiment at Max Planck Institut für Quantenoptik (MPQ), using the Asterix laser source which can deliver up to 300 J laser energy per pulse in 0.45 ns. Also, we used different biological specimens, in order to image cells with different transmission characteristics as a test for the contrast, and with fine details, so that the theoretical resolution limit of this technique could be tested.

In this paper we describe our experiment and the results, concerning both the characterisation of the plasma source and the quality of images obtained with various biological samples. The experimental set-up is presented in Section 2, while in Section 3 we describe the biological samples; Section 4 is devoted to the discussion of the limiting factors of SXCM, and Section 5 to the presentation of the experimental results. Finally, Section 6 contains the concluding remarks.

2 Experimental set up

The experimental set-up is sketched in Figure 1, where the interaction chamber, the laser path and the main diagnostics are shown. In this section we describe it in detail.

2.1 The laser source

ASTERIX is an iodine laser operating at a wavelength of 1.314 μm converted in the third harmonic (0.438 nm), whose pulse is characterised by a Gaussian temporal shape, with a FWHM of 0.45 ns. The laser beam, which has a diameter of 30 cm, has been focused by means of a $f/2$ lens ($f = 564$ mm) onto the targets; the residual fundamental and second harmonic radiation, which would have been defocused due to the absence of a chromatic correction in the lens, has been eliminated by means of a blue filter, therefore avoiding the increase of debris. The typical value of the pulse energy was about 250 J; the intensity on target was between 2×10^{14} and 2×10^{15} W/cm^2, the focal spot varying between 650 and 200 μm.

2.2 The X-ray source

The X-ray emitter is a foil heated by the laser; the hot coronal plasma which is formed on the surface is the source of the radiation, with a spectrum which is characteristic of the target element; in general low Z materials produce simple K-shell spectra, while high Z targets are characterised my more complex ones [13,14]. We used targets made of carbon (plastic), boron nitride, yttrium, zirconium, molybdenum, or gold.

High Z materials produce an X-ray spectrum less clean than that of low Z ones, and in principle less favourable for SXCM; however, low Z elements have also a low conversion efficiency from laser to X-ray energy, resulting in lower fluxes in the WW. The emitted spectrum also depends on the laser intensity, X-rays being harder for higher intensities (*i.e.* higher plasma temperatures).

2.3 Diagnostics

Source characteristics (dimension and time duration, absolute flux) were diagnosed by means of several devices. Once more, we want to stress that the high flux provided by ASTERIX allowed the use of single shot diagnostics, and enabled us to keep the samples far away from the source, therefore leaving enough room to simultaneously place several diagnostics and/or multiple specimen holders in the chamber.

A pin-hole camera coupled to a transmission grating spectrometer [15] (1 000 lines/mm) allowed us to measure the focal spot diameter in different spectral regions. The images were registered on Ilford Q-Plates, and the part of the spectrum corresponding to the WW was 880 μm long on the film; this was analysed by means of a microdensitometer with a resolution up to 1 micron, therefore enabling us to obtain information about the dimension of the emitting source at different wavelengths. We used an X-ray streak camera with a gold cathode [16], coupled to another transmission grating (5 000 lines/mm), in order to time resolve the spectrum of the X-ray source. Due to the higher spectral resolution of this device (of the order of 0.1 nm), it was possible to compare the total emissions in the WW region and at energies ranging from the oxygen absorption edge to 4 keV by taking into account the sensitivity of the streak camera at the different wavelengths.

Vacuum photo diodes and PIN diodes were used to measure the absolute X-ray flux, allowing us to evaluate the conversion efficiency for the different materials. In particular, two PIN diodes (Quantrad Sensor 100-PIN-125) were mounted at the end of a 1.5 m long tube installed on the interaction chamber; the need for such a distance from a source was to avoid saturated signals. These diodes were coupled respectively with aluminium filters, whose thickness were chosen in the interval 20–70 μm in order to take into account the expected X-ray emission, and with a copper mirror and a vanadium filter 0.5 μm thick. In this way, one diode was able to detect photons with energies in excess to 1 keV, while the other could select photons at energies below 860 eV. To obtain the data on the X-ray

Table 1. Ratio between the energy fluxes due to WW photons (E_{WW}) and harder photons (E_h) for a zirconium target and different spot sizes.

Spot size (μm)	E_{WW}/E_h
200	1.8
400	4.1
600	10.2

flux in these energy ranges, we have processed the experimental signal by assuming a flat X-ray spectrum in the respective spectral windows. Since in reality the X-ray flux depends on the detailed spectral shape, these results are mainly qualitative. However they are useful to compare the X-ray emission in the WW and at shorter wavelengths from various target materials. Their main utility was that PIN diodes allowed a faster characterisation of the shot than the X-ray streak camera, hence usable in "real time" during the experiment. Some results are shown in Table 1.

Finally, calorimetric diagnostics provided the information on the laser pulse energy for each shot.

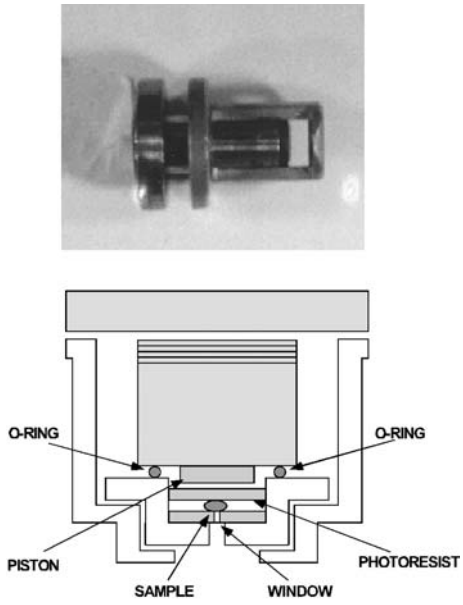

Fig. 2. Sample holder.

2.4 Interaction chamber

The ASTERIX interaction chamber was octagonal in shape, with a flat removable vertical plate on each side. Its easy access allowed us to change the targets and the sample holders very quickly, and its large dimension were sufficient to host up to twelve holders per shot on the ground plate. In this way, we could check the reproducibility of SXCM taking images of different samples at the same time, under the same experimental conditions; we could also obtain images of the same samples placing the holders at different distances, hence varying the X-ray flux, while leaving all the other parameters unchanged. Having multiple exposures of the same specimens produced under identical imaging conditions also provided replicates upon which different photoresist development conditions could be investigated. Also the statistics could be improved thanks to the larger number of obtained images.

The chamber was evacuated by a turbomolecular pump down to 10^{-4} mbar in less than 30 min of pump time. The necessity for such a low pressure comes from the requirements of the X-ray streak camera (XRSC-II system, developed at the Max Planck Institute für Quantenoptik [16]), while 10^{-2} mbar would be sufficient for SXCM. A fast evacuation time is necessary to avoid stress or death of the biological cells in the holders.

2.5 Sample holders

The sample holders (Fig. 2) have been designed to avoid the evaporation of the water solution containing the biological specimen during the pumping of the interaction chamber, and to hold the photo resist used to produce the images (we used polymethylmetacrylate, PMMA).

The holders were cylindrical in shape (35 mm high and 25 mm in diameter) and had on the top a window made of silicon nitride [17] 100 nm thick, which has a relatively high transmission (about 60%) in the WW region. A drop of the solution containing the cells was placed between the window and the PMMA. Since silicon nitride is transparent to visible light it allowed us to view the cells under a light microscope whilst tightening micrometric screws to reduce the space between the window and the photo resist to a minimum (the cell diameter), reducing the water thickness; in this way it was possible to maximise the amount of X-rays used to form the image. This allowed also to avoid, in most of the cases, the cells to overlie one another; moreover it allows reproducible conditions to be obtained (however this is really a still partially unsolved problem, because the pressure of water on the window forces it to bend, so that the water thickness is not uniform across the whole imaged area and it is difficult to adjust it in the same way for different sample holders).

The careful and quick preparation of samples was very important, because some specimens may suffer or hardly survive within the holders due to factors such as oxygen deprivation. In particular sperms cannot survive longer than 30 minutes inside a holder, while yeast cells are more resistant. We exposed up to 12 sample holders per shot and we took care in preparing yeast cells first and the weaker specimens later, thereby reducing the risk of imaging dead or stressed cells.

2.6 Atomic force microscope

For each sample the development time was experimentally varied in order to get the best image. After the development, the photoresists were analysed using Atomic Force Microscope (AFM): we used a Park Scientific SA or a Burleigh Personal AFM. The images obtained from the

biological samples show a density pattern of the cells in which the lighter zones correspond to those denser in carbon, due to the higher absorption of the X-rays.

The Park SA uses a piezoelectric system to detect the deflection of the cantilever, therefore avoiding all the problems due to the time consuming procedures of alignment of other systems. Moreover, it can operate in non-contact mode, keeping the tip in vibration very close to the sample, without touching it. In this case, the feedback circuit is locked on vibration amplitude, rather than on cantilever deflection. The non-contact mode analysis allows to see the dust which is sometimes present on the photo resist, avoiding problems such as the loss of some scan lines or the loss of contact; in particular, the loss of contact forces the analysis to restart, increasing the time required for each sample.

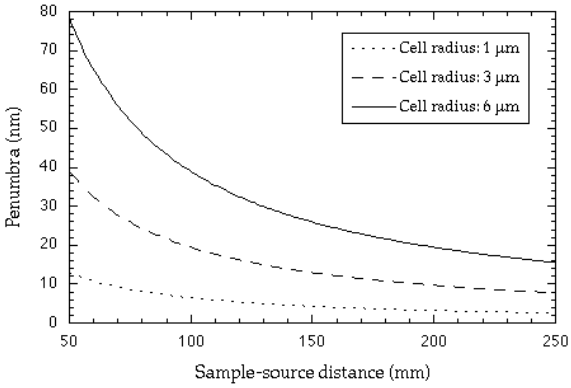

Fig. 3. Dimensions of the penumbra (in nm) *vs.* distance sample-source in the case of three different cell radii; source dimension: 650 μm.

3 Biological samples

Biological samples were chosen with different characteristics of cell wall thickness and presence of fine details. They were *Saccharomyces cerevisiae* (yeast cells), *Chlamydomonas* (a unicellular green algae), *Phytomonas, Crithidia, Human Red Blood Cells, Pig Sperm*, and *Trout Sperm.* All specimens mounted in water.

Yeast cells are characterised by a thick, carbon rich, cell wall (∼200 nm), which strongly absorbs X-rays in the water window region, making it difficult to observe internal details and potentially producing low contrast images, for this reason they are a good test for the capability of this technique to image "thick" samples. Previous attempts to image yeast cells with a low energy source were indeed rather unsatisfactory, showing few details of their inner structures [18].

In comparison, *Chlamydomonas* have thinner cell walls (∼10 nm), allowing easier imaging of the inner organelles. In this way, the combined use of yeast and *Chlamydomonas* represents a good test for contrast in SXCM [19].

Flagella in *Chlamydomonas* and pig sperm cells provide a way to check the spatial resolution of the technique. In particular, EM has shown that sperm flagella contain nine couplets of micro tubules (doublets) in the neck (*i.e.* the part attached to the head of the cell), each of them about 25 nm in diameter [20,21]; therefore a doublet is at the theoretical limit (50 nm) of SXCM.

4 Limiting factors of spatial resolution

Two main factors reduce the spatial resolution of the SXCM, *i.e.* penumbral blurring and Fresnel diffraction [5,9].

4.1 Penumbral blurring

Penumbral blurring (p) is due to the finite size of the X-ray source, and depends also on the dimension of the imaged object and its distance from the source and the photo resist. It can be calculated as (with $d \ll D$):

$$\rho = d\left(\frac{S}{D}\right) \tag{1}$$

where d is the distance between the sample and the photo resist, D is the distance between the source and the sample, S is the source diameter. In our case, the lowest distance between the source and the holders was more than 5 cm, while we can estimate d to be of the order of the cell diameter, that is ∼6 μm for the largest ones. As said in the section about the laser source, the largest focal spot was 650 μm (as measured with the pin-hole camera), which implies that the penumbral blurring sets a resolution limit less than 80 nm. It must be noted, however, that indeed this is the worst case, since finer details could be obtained if smaller size parts, such as flagella, were in close contact with the photo resist or for smaller focal spots and larger distances.

Again, the use of a high intensity systems allows to place the holders far away from the source, minimising this problem.

Plots of p *vs.* D for a 650 μm wide source and three different cell radii (assumed to be equal to d) are shown in Figure 3.

4.2 Fresnel diffraction

The resolution limit due to Fresnel diffraction is given by [22]:

$$f = (\lambda\,(d_1 + d_2))^{\frac{1}{2}} \tag{2}$$

where λ is the radiation wavelength, d_1 is the distance between the sample and the photo resist (of the order of the cell diameter) and d_2 is the development depth of PMMA. Typical values of d_2 are less than 100 nm, so d_2 can be neglected in this formula ($d_2 \ll d_1$). The blurring due to Fresnel diffraction is of the order of 130 nm with yeast

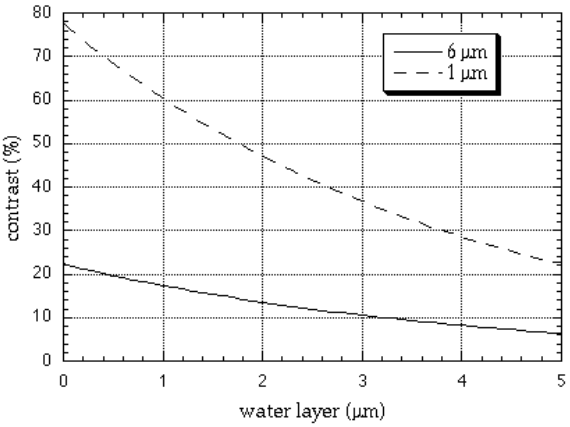

Fig. 4. Contrast reduction as a function of the thickness of a water layer above yeast cells with diameters of 6 μm and 1 μm.

cells, which have a diameter of about 6 μm and a radiation wavelength of about 3 nm. However, as for penumbral blurring, we expect a lower value for other samples, because of the smaller dimensions and closer distances to the PMMA. Moreover, for all biological samples the use of formulas based on Fresnel diffraction will yield an overestimation of blurring, since, in our case, the specimens are not completely opaque to the incident X-ray radiation.

Hence in our experimental conditions the minimum resolvable details are expected to be of the order of 50 nm, an evaluation which has been confirmed by experimental results (see, for instance, Fig. 17a).

4.3 Contrast

An important limiting factor is the loss of contrast due to the absorption of X-rays produced by a water layer placed above the cell or between the cell and the resist.

We can evaluate the contrast between a region irradiated by X-rays which have crossed a water layer of thickness x_1 plus a cell of thickness x_2, and those which have crossed a water layer of thickness x_1+x_2. If we neglect the absorption due to the silicon nitride window (about 30% to 40%), the difference in the two numbers of photons is given by:

$$\Delta N_{\mathrm{PMMA}} = N_x \exp[-\mu_{\mathrm{w}}(x_1+x_2)] \times \{1-\exp(-\mu_{\mathrm{w}}x_1-\mu_{\mathrm{c}}x_2)/\exp[-\mu_{\mathrm{w}}(x_1+x_2)]\} \quad (3)$$

where N_x is the total number of incident photons, μ_{w} and μ_{c} are the linear absorption coefficients of the water and of the cell. Defining $C = \Delta N_{\mathrm{PMMA}}/N_x$, we get:

$$C = \exp[-\mu_{\mathrm{w}}(x_1+x_2)][1-\exp(-\mu_{\mathrm{c}}+\mu_{\mathrm{w}})x_2]. \quad (4)$$

In order to have a high contrast it must be $\mu_{\mathrm{c}} \gg \mu_{\mathrm{w}}$ and $\mu_{\mathrm{w}}x_1 \ll 1$, that is if the water layer above the cell is small. A graph showing the contrast C as a function of the water layer is shown in Figure 4; in this case we have considered a radiation with $\lambda = 3.27$ nm, $\mu_{\mathrm{w}} = 0.25\ \mu\mathrm{m}^{-1}$ and $\mu_{\mathrm{c}} = 6.3\ \mu\mathrm{m}^{-1}$ [23], and two yeast cells, respectively 6 and 1 μm in diameter, which for sake of simplicity have been supposed to be made just of carbon. It is worth noticing how the presence of a few microns of water can strongly reduce the contrast, and how this is higher for smaller objects, as in this case, the absorption due to water layer x_2 is also lower.

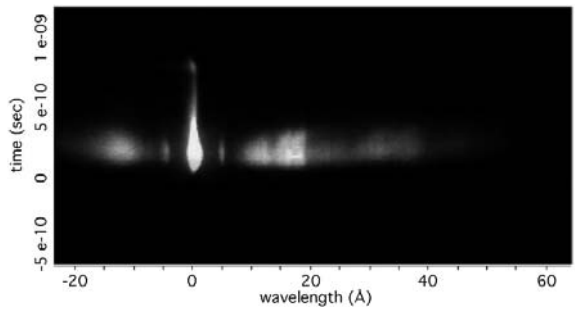

Fig. 5. Time resolved emission spectrum of a molybdenum target taken with the X-ray streak camera coupled with the 5 000 lines/mm grating. Time flows upwards. The elongated feature on the left is the zero order image of the source.

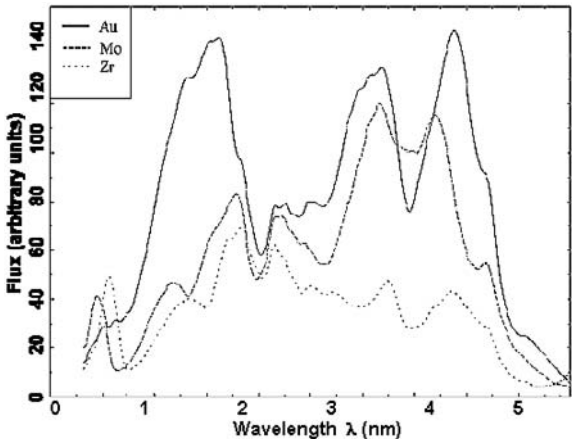

Fig. 6. Emission spectra of gold, molybdenum and zirconium targets taken by the streak camera. The profiles correspond to the time of the maximum X-ray emission for each shot.

5 Results

5.1 X-ray spectra

The X-ray streak camera provided the time resolved X-ray spectrum for each shot, so that we could compare the emission of each different target.

We could see, at the same time, the water window, the softer and the harder X-ray regions.

Figure 5 shows an image obtained with the streak camera using a molybdenum target. Time flows from the bottom to the top of the image, while the horizontal axis contains the spectral information; the spectrum is symmetric around the zero order image given by the grating.

In Figure 6 we compare emission spectra from gold, molybdenum and zirconium. The plots correspond to the

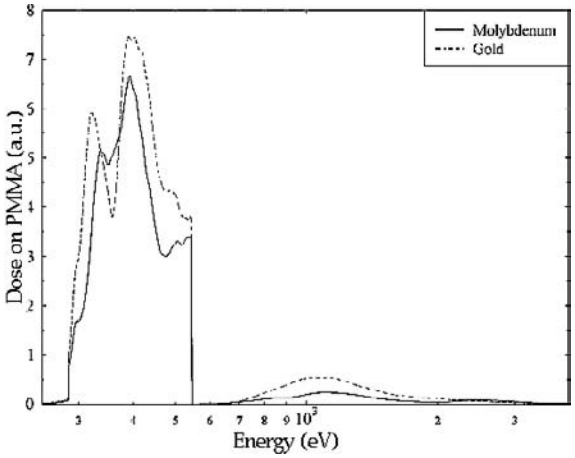

Fig. 7. Energy absorbed by 100 nm of PMMA after 5 μm of water in the case of molybdenum (continuous line) and gold (dashed line). The low sensitivity of the PMMA to high energy radiation greatly reduces the differences in the absorbed spectrum.

spectral emission obtained at the time in which the laser intensity reaches its maximum value on target, and have been computed taking into account the spectral sensitivity of the streak camera.

Zirconium shows a lower flux within the water window than other emitters, but, in our experimental conditions, it was sufficient to get high quality images of biological specimens.

Gold and molybdenum have nearly the same flux within the water window. However gold has a stronger emission in the 0.5 to 1 keV region and, for this reason, it does not seem to be optimal for SXCM.

The choice of the spectrum affects image contrast. In principle this is reduced by hard X-rays, for which both water and carbon are almost equally transparent. Since we had high laser intensities and high Z targets, we obtained high X-rays flux, but also spectra which extend far beyond the WW. The choice of larger focal spots used in some shots was made to get a lower intensity and a lower plasma temperature; this could be of some advantage, implying a lower X-ray emission at high photon energy without appreciable loss in resolution thanks to the large sample-source distance obtainable with Asterix.

Contrast loss due to hard X-rays is often considered a major problem in the literature. However, if we consider the radiation produced from different targets and absorbed by 100 nm of PMMA (*i.e.* the amount of photo resist which is usually removed by the chemical development) after a 5 μm water layer, we can show (see Fig. 7) that there is little absorption by PMMA in the 1 keV region and that the difference between gold and molybdenum is negligible; the sharp fall after 500 eV is due to the absorption edge of oxygen, which is present both in water and PMMA. This means that in reality image quality and contrast will not be drastically affected by hard X-ray photons. In other words, since these are not strongly absorbed by PMMA, they spread through a large PMMA thickness giving a low effective irradiation. This is due to the strong absorption of water at energies just above the WW, and to the low sensitivity of the PMMA at higher energies.

The results shown in Figure 7 have been obtained by calculation: absorption at specific wavelengths has been calculated using Henke's tabulated absorption coefficients [23], and the chemical composition of water and PMMA. Indeed, our biological images do not show appreciable differences when using targets like gold or molybdenum, in agreement with the above discussion.

Finally, we want to stress the fact that the use of a high intensity laser produced a high incident X-ray flux on the photo resist, therefore increasing the total signal, which turned out to be a benefit in analysing the images. In fact, although theoretically the difference in absorption between "transparent" and "opaque" regions in the sample is independent of X-ray flux (absorption is linear), in practice only a sufficient X-ray irradiation can give a good signal-to-noise ratio. The absence of high contrast, rather than a reduced resolution, may indeed be the cause for the failure of imaging very thin structures in other SXCM experiments (see next paragraph). The use of a high energy laser source proves to be useful with this respect too.

5.2 Image quality

In the following analysis of the influence of the different parameters on image quality we will consider images obtained by changing only one parameter at a time, so that its influence on image quality can be fully evaluated.

5.2.1 Sample-source distance

The sample-source distance has, *a priori*, two effects: larger distances will indeed correspond to a lower penumbral blurring (improved resolution) but also to a lower X-ray flux on the sample.

A first comparison is made in Figure 8, where we present two blood red cells placed respectively at a distance of 8 cm and 12 cm from the X-ray source (polypropylene target). No appreciable differences can be observed in the two pictures. Although the difference between 8 and 12 cm may appear small, it corresponds to a variation $(12/8)^2 \sim 2.25$ in X-ray flux.

Figures 9a and 9b show two yeast cells (zirconium target, 400 μm wide focal spot) placed respectively at a distance of 5 and 7.5 cm. In this case, the best image is the one corresponding to the lower distance, where the cell wall can be recognised. Here the higher X-ray flux may have been the crucial factor in producing the better result.

In Figure 10 we compare two *Chlamydomonas* cells, both imaged with a zirconium target (400 μm wide focal spot). Figure 10a has been obtained from a sample placed at 10 cm, while the cell in Figure 10b was 20 cm far from the source. No internal details can be observed in either pictures, while flagella can be viewed only in Figure 10a.

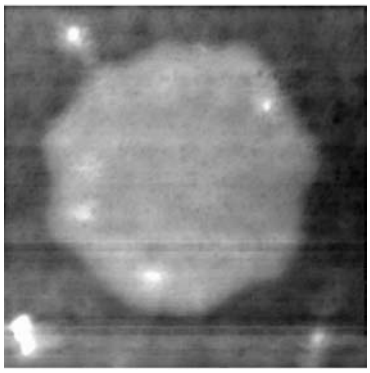

(a)

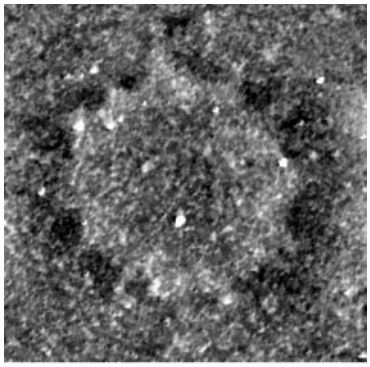

(b)

Fig. 8. Blood red cells placed at 8 cm (a) and 12 cm (b) from the source (polypropylene).

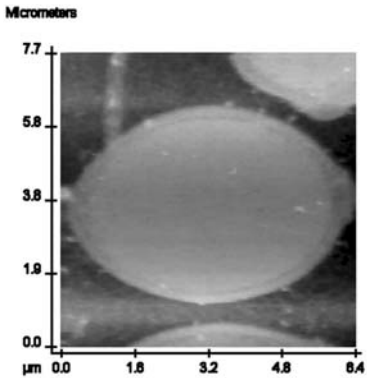

(a)

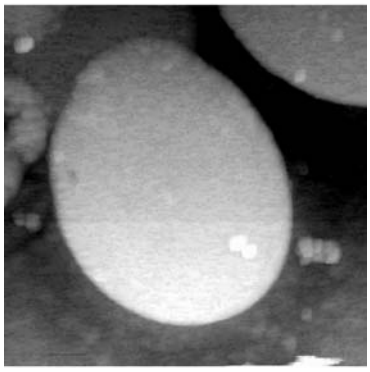

(b)

Fig. 9. Yeast cells imaged using a zirconium target and a focal spot of 400 μm. The cell in (a) was placed 5 cm from the source, while that in (b) was at a distance of 7.5 cm.

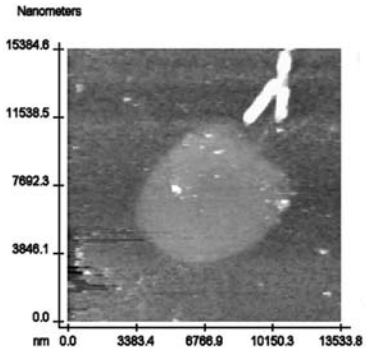

(a)

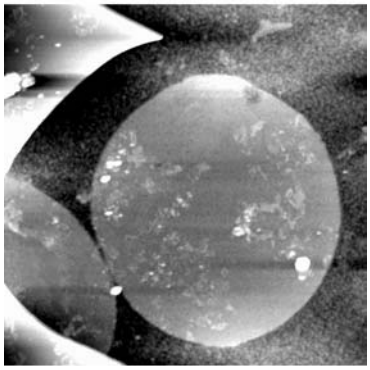

(b)

Fig. 10. *Chlamydomonas* algae. The source is the same of Figure 8, distances of 10 and 20 cm in (a) and (b) respectively. The bright spots in (a) are two bacteria.

The difference in X-ray flux is here ∼4, however it must also be noted that in the case of Figure 10b the cell was placed near the centre of the photo resist, where the water layer is larger due to the bending of the silicon nitride window, and therefore the quality may be reduced also by the higher absorption. The two bright spot on the upper right corner of Figure 10a are bacteria.

Two yeast cells are shown in Figures 11a and 11b, placed respectively 10 and 15 cm far from the source. We used a gold target and a focal spot of 600 μm. In this case we see that Figure 11a is of a higher quality than Figure 11b, since a larger amount of details are visible: the cell wall and areas differing in X-rays absorption in the cytoplasm are clearly imaged in this picture. Also, some budding is evidenced in both cells. It must be noted that some small holes are present on the photo resist, and are viewed as small dark spots in (a), while granulation in (b) is due to the dirty surface of the photo resist.

In Figure 12 we compare two images of yeast cells obtained with a molybdenum target and a focal spot of 650 μm; the distance of the samples from the source was respectively 15 and 20 cm in the cases (a) and (b). The first image is better than the second, since it clearly shows the cell wall and the cytoplasm.

The four pictures in Figure 13 show some yeast cells; the images were produced with an yttrium target and a source diameter of 600 μm at distances of 7, 8, 10 and 15 cm from the target. The best quality is obtained in Figures 13c and 13d, where the cell wall and some internal structures may be observed.

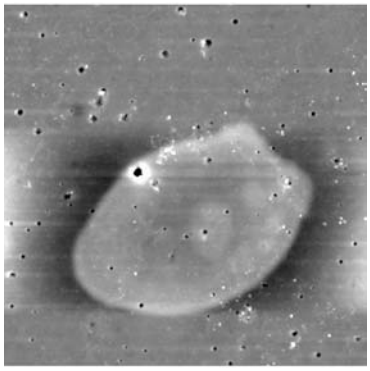

(a)

(b)

Fig. 11. Yeast cells imaged using a gold target, a focal spot 600 μm wide and distances equal to 10 cm (a) and 15 cm (b). The budding process is present in both samples, as evidenced by the two protrusions on the edge of the cells.

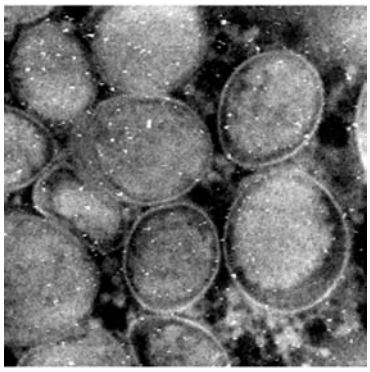

(a)

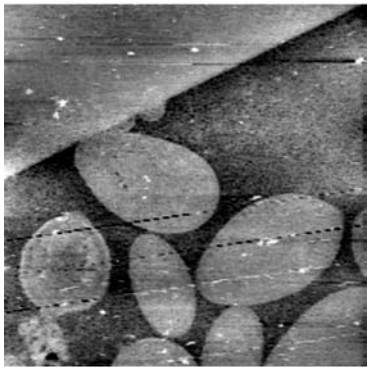

(b)

Fig. 12. Two yeast cells images taken with a molybdenum source (focal spot diameter of 650 μm; the distance of the samples is 15 cm in (a) and 20 cm in (b)). Shrinking of the cytoplasm in (a) indicates that the cells may be stressed.

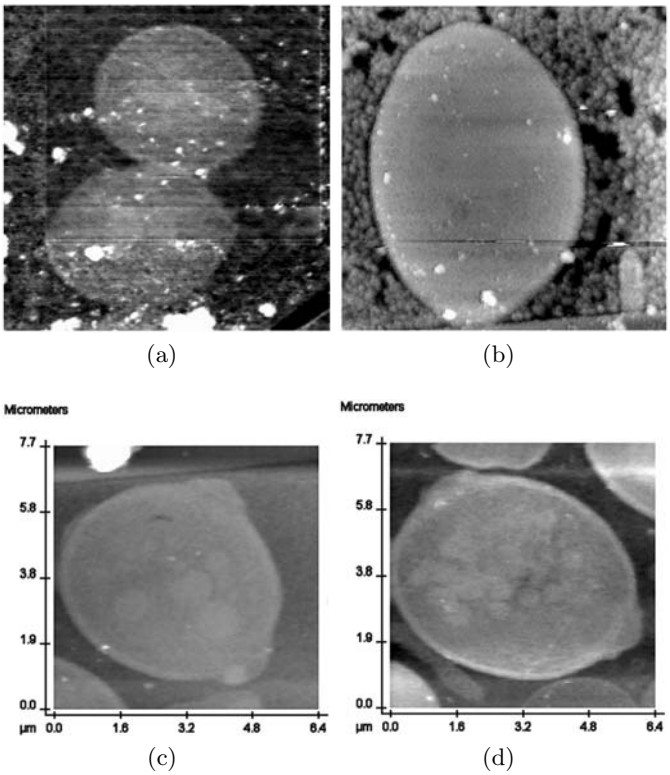

(a) (b) (c) (d)

Fig. 13. Four images of yeast cells obtained with a 600 μm wide source of yttrium. Distance from the source is 7 cm in (a), 8 cm in (b), 10 cm in (c) and 15 cm in (d). The best quality has been achieved in (c) and (d), where internal details can be observed. Notice also the budding taking place in (c) and (d).

The comparison between images taken at different distances from the source allows us to conclude that the best images appear to be produced when the specimen was placed between 10 and 15 cm from the source. Probably photo resists placed too close to the target may be damaged in some way and produce images with lower quality. On the opposite side, samples which are too far from the source may receive too few X-rays, which can be a disadvantage especially in the case of yeast. Finally, we observe that in our experimental conditions penumbral blurring does not produce significant effects even at the shortest distances, since resolution appears to be comparable in corresponding images obtained at different distances.

5.2.2 Target material

The next issue of this work is to analyse the dependency of the image quality on the target material, *i.e.* on total flux and the spectral characteristics of the X-ray source. *A priori* we expect better images to be obtained with targets which give a higher flux in the WW.

In Figure 14 we can see several yeast cells, which were placed 20 cm far from the source (650 μm diameter): Figure 14a was obtained with a gold target, while in

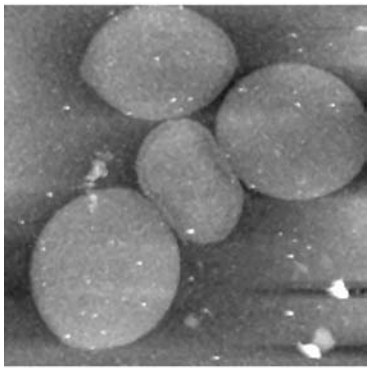

(a)

(b)

Fig. 14. Clusters of yeast cells. In both images the distance from a source 650 μm wide was 20 cm; in (a) the target was gold, while in (b) it was molybdenum.

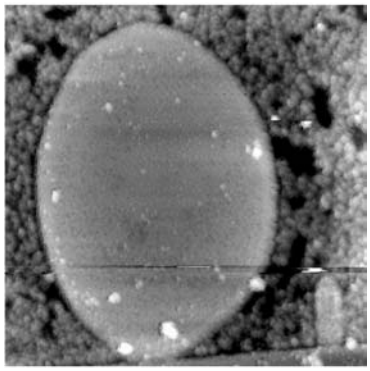

(a)

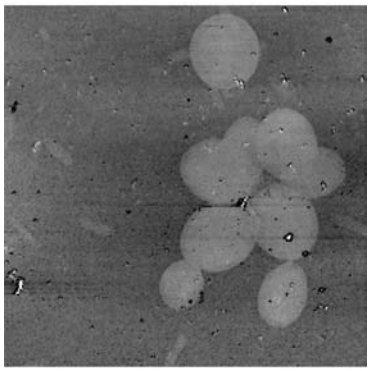

(b)

Fig. 15. Images of yeast cells obtained with sources of 600 μm diameter; yttrium target, 7 cm distance in (a), zirconium target, 8 cm distance in (b). The clustering in (b) is due to the position of the cells, close to the centre of the photo resist, where the water layer is thicker.

Figure 14b we used molybdenum. The average quality of both images is quite low, due to the large distance, however, Figure 14b shows a larger number of internal details.

In other images of yeast cells, in Figure 15a (yttrium target, 600 μm focal spot, 7 cm distance) and (b) (zirconium target, 600 μm focal spot, 8 cm distance) show no internal details, nor significant differences from each other. The superposition of cells in Figure 15b indicates that they were clustered in a region where the water layer was rather thick, therefore potentially reducing the quality of the picture.

Figures 16a and 16b again show some yeast cells; they were placed at a distance of 10 cm from the source using respectively an yttrium and a gold target, with a focal spot of 600 μm in both cases. Also Figure 17 shows yeast cells (Y target in (a), Au target in (b), focal spot of 600 μm), but in this case the distance from the source was 15 cm.

Both in Figure 16 and in Figure 17, yttrium shows better results than gold. In general, we have noticed that yttrium and molybdenum provide a better X-ray source than gold for imaging biological material.

5.2.3 Biological samples

We now examine the images of different biological samples taken under the same experimental conditions. Of course, in this case the analysis is more complicated, as the specimens differ in fine details and in absorbing properties.

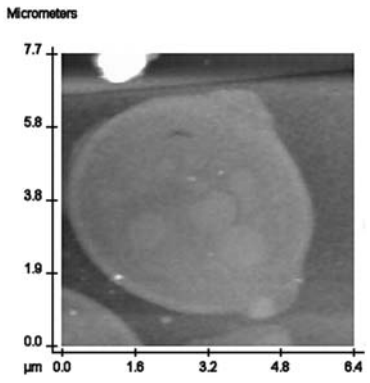

(a)

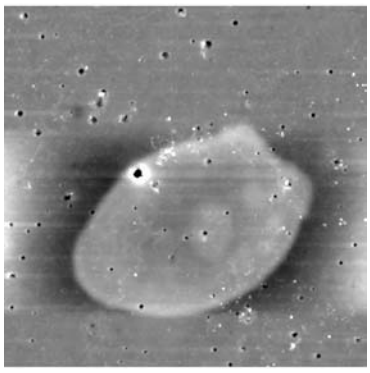

(b)

Fig. 16. Yeast cells imaged using an yttrium (a) and a gold (b) target, a focal spot of 600 μm, and placing the samples 10 cm from the source.

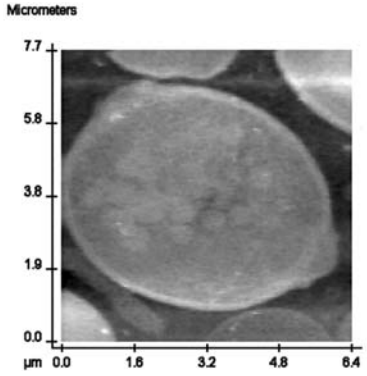

(a)

(b)

Fig. 17. Yeast cells. Target and focal spot as in Figure 15; in these images the distance from the source was 15 cm.

A priori we expect thinner samples to show internal details more easily even at bigger sample-source distances, while thicker samples (like yeast) will need higher fluxes and shorter distances. In general, we can also gain information on the best conditions for each different kind of sample.

A molybdenum target was used for the pig sperm cells and the yeast cells in Figures 18a and 18b respectively (650 μm focal spot, 15 cm distance). The images of sperm are really interesting, as doublets can be seen in the region where the flagellum is connected to the head in the sperm cells; these structures measure 50 nm in diameter, being therefore at the theoretical limit of this technique. Also the yeast cells show a large number of internal details.

Figure 19 compares a *Chlamydomonas* (a) and two *Crithidia* (b) cells. We took these images using a zirconium target placing the samples at a distance of 10 cm from it, the focal spot being 400 μm in diameter. The quality of both images is high, the two flagella being clearly observable as are the typical cytoplasmic spheres in the *Chlamydomonas* cells, and several structures in the *Crithidia*.

From this comparison, we can conclude that, under the same imaging conditions, different samples can give images of comparable quality, even if the biological characteristics are quite different, as in the case of yeast and sperm cells. Again, a crucial factor is the thickness of the water layer between the sample and the window, which may alter the quality independently from other parameters (target material, sample-source distance).

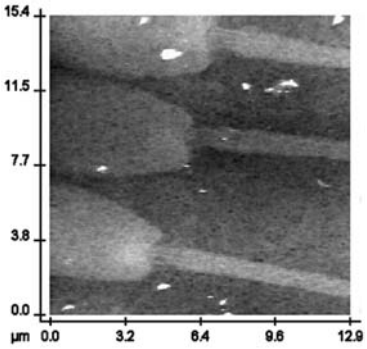

(a)

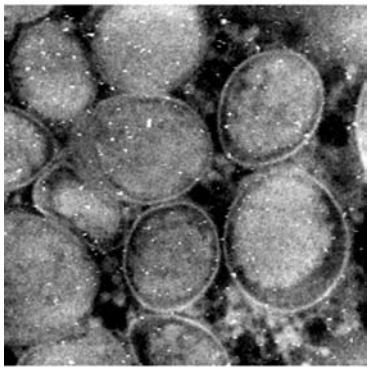

(b)

Fig. 18. Pig sperm (a), and yeast cells (b) images obtained with molybdenum. Focal spot of 650 μm, distance 15 cm. In (a) fine structures at the resolution limit of this technique (50 nm) can be viewed: these are the doublets in the neck of the cells.

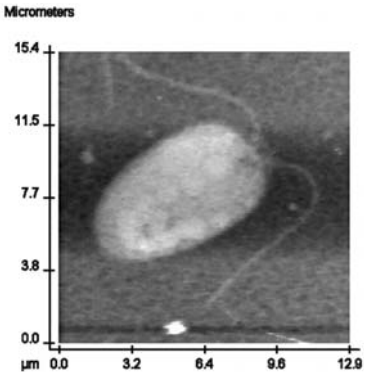

(a)

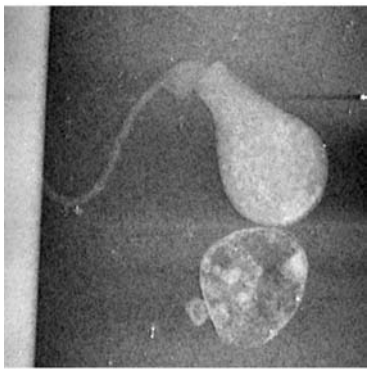

(b)

Fig. 19. A *Chlamydomonas* cell with two flagella (a), and two *Crithidia* cells (b) at different stages: the top one with flagellum and thicker cell wall is younger than the bottom one, which, due to the thinner wall, shows some internal details. The target material was zirconium, with a focal spot of 400 μm and a distance of 10 cm. The *Chlamydomonas* in (a) shows internal cytoplasmic spheres.

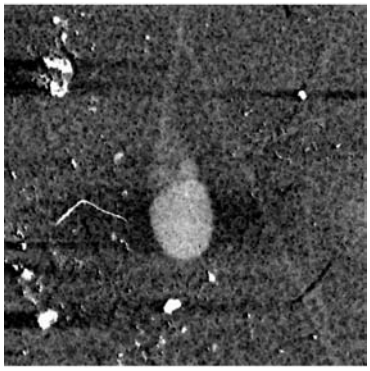

(a)

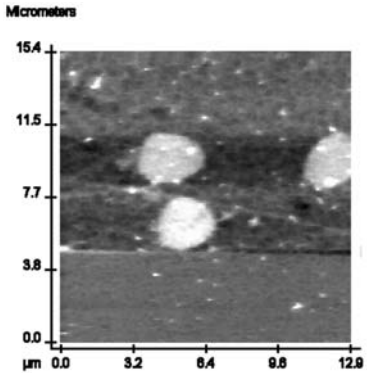

(b)

Fig. 20. Trout sperm cells (Zr target, 250 μm focal spot); the distance between the target and the sample was 15 cm in (a) and 16 cm in (b).

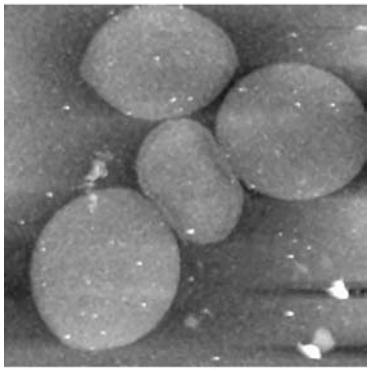

(a)

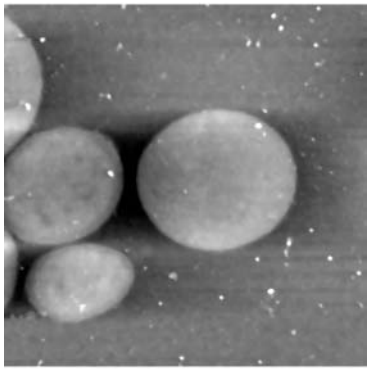

(b)

Fig. 21. Yeast cells placed 20 cm ((a) and (b)) and 18 cm (c) from a gold target (focal spot 650 μm wide).

5.2.4 Reproducibility

Finally, we consider the case in which the images were obtained under the same conditions, in order to test the reproducibility of the results.

In Figure 20 we show two images of trout sperm cells produced by a zirconium target; the focal spot was 250 μm wide, and the holders were placed at a distance of 15 and 16 cm respectively, which can practically be considered the same. The cell in Figure 20a shows a better definition of the head and also a brighter area at the base of the flagellum; this is a mytocondrium, an organelle which provides the energy necessary for the movement of the flagellum. On the other side, the cells in Figure 20b lack in details, even if the flagella are visible. The difference in quality may be due, in this case, to a thicker layer of water in the second case.

A similar comparison is made in Figure 21, where two groups of yeast cells are imaged; in all cases, a gold target was used, with a focal spot of 650 μm, and a distance of 20 cm between the source and the samples for Figures 21a and 21b, and 18 cm for Figure 21c. No significant differences can be appreciated in the images, although some finer details can be viewed in Figure 21a (the wall of the cell in the centre of the picture), and the low quality of Figure 21c is due to dirt on the resist. A possible cause for this can be the large distance between the samples and the source, and therefore an insufficient X-ray flux, unable to penetrate effectively inside the thick cell wall of the yeast cells. However, the most important point is the comparable quality of the two images.

Finally, in Figure 22 we show some blood red cells placed 8 cm far from a polypropylene (carbon) target (focal spot of 400 μm). Even in this case the image quality is comparable in the two cases. The cells show a strange shape due to the fact that they were not placed in an isotonic solution, and therefore they will have taken up excessive water by osmosis and may even have burst under the effect of the increased internal pressure.

As a conclusion we can say that SXCM images obtained in the same conditions (and with the same biological sample) give images which are usually of comparable quality. However this is not always the case (as seen in Fig. 20, for instance). Here the crucial point, as already said, seems to be the control of the water layer thickness in the sample holder. In all cases, images of cells close to the centre of the photo resist (where the water layer is thicker) are of worse quality.

5.3 Biological results

In this section we discuss the biological results, giving a special emphasis to the main achievements obtained in our experiment. As observed in the previous section, we could get interesting images for several specimens.

Despite the thick, dense wall of the cells, the images of yeast cells have provided reliable measurements of the

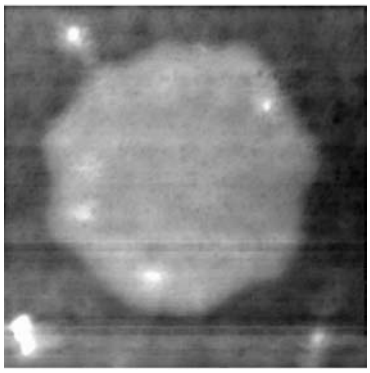

(a)

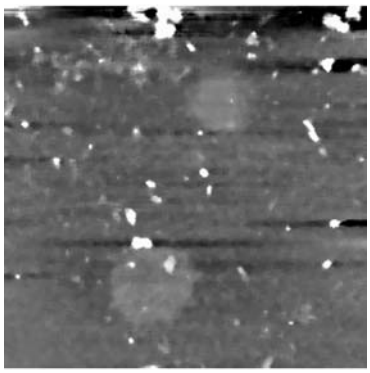

(b)

Fig. 22. Blood red cells (polypropylene target, 400 μm focal spot, 8 cm distance). The cell shapes indicate that the cells have burst due to improper osmolarity of the solution.

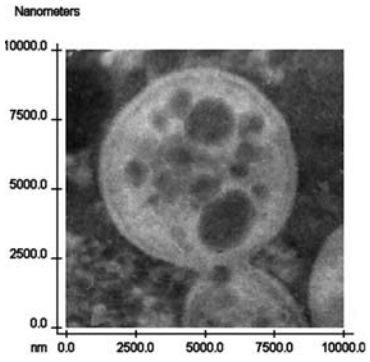

Fig. 23. A yeast cell in the final stage of budding. The cell wall and vacuoles are clearly imaged.

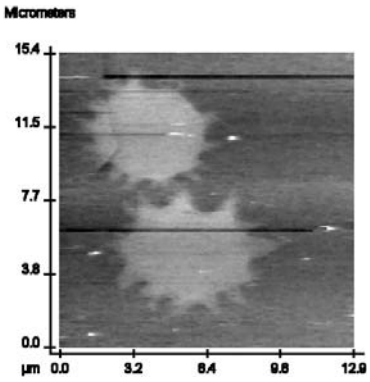

Fig. 24. Two blood red cells bursting under the effect of internal pressure.

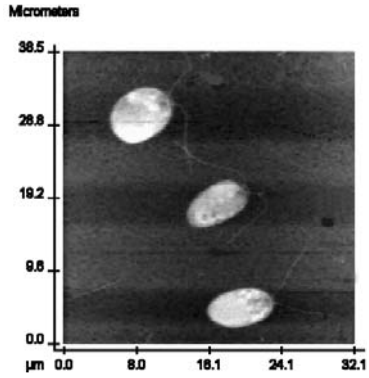

(a)

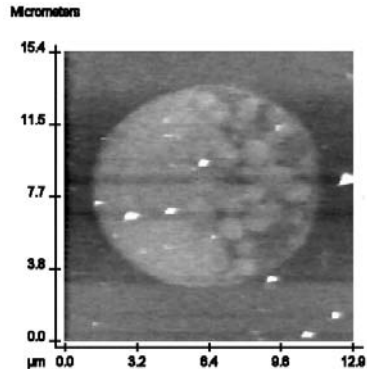

(b)

Fig. 25. *Chlamydomonas* cells: the three in (a) show flagella and spheres, while in (b) the flagellum is not visible due to the orientation of the cell.

cell wall, and also some details in the cytoplasm, such as the vacuoles, which have been successfully imaged (as in Figs. 12–14). The quality of these images is comparable with that obtained with TEM [24] although the information obtained is different. However, we could notice some damage to cells as evidenced by a shrinking of the cytoplasm away from the cell wall (Fig. 12a).

In two cases (Fig. 11) we recorded images of budding cells showing two protrusions on opposite sides, when this process is still in the initial stages (this also indicates synchronous multiple budding from the same cell).

The yeast cell in Figure 23 shows plenty of detail: the cell wall is well defined, and several low density (dark) patterns appear in the cytoplasm which probably represent vacuoles or other organelles with contents of lower carbon density that the surrounding cytoplasm. Also, on the lower right corner, budding in its final stage is seen. The image was obtained with a molybdenum target, and the sample was placed at a distance of 15 cm from the source.

The blood red cells in Figure 24 show a distorted shape due to the fact that they were not placed in an isotonic solution, and therefore are bursting due to the increased internal pressure.

Pig and trout sperm (respectively Figs. 18a and 20) and *Chlamydomonas* (Figs. 10a, 19a and 25a) cells have shown that the flagella, and also some of the internal structures are clearly recognisable. In pig sperm the thin doublets between the flagellum and the head of the cell, which are at the limit of resolution of the technique, can be seen (Fig. 18), while a mytocondrium is observable in the image

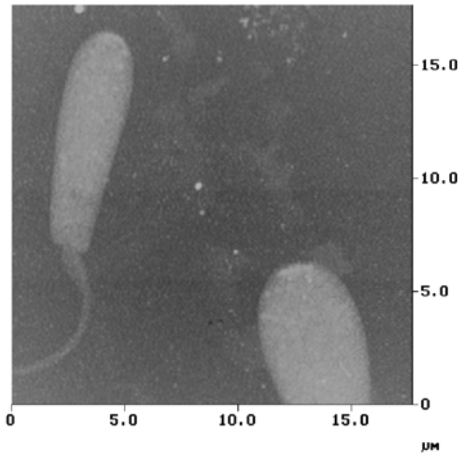

Fig. 26. A cell of *Phytomonas* showing the flagellum and different absorbing areas in the cytoplasm.

of a trout spermatozoon (Fig. 20a). The images of *Chlamydomonas* (Figs. 19a and 25) show some special structures which have been observed before in SXCM, but which are not imaged by electron microscopy (insert ref).

Figure 19b contains two *Crithidia* cells: they show a different morphology due to the different developmental stages of the cells. The upper one is in fact a young cell with a flagellum and a thick membrane which does not allow inner structures to be clearly imaged; the one on the lower side of the picture, instead, is an old one, whose thinner wall reveals several internal details.

The *Phytomonas* in Figure 26 show the flagellum and the rather carbon-dilute cytoplasm of the cell is clearly visible.

6 Conclusions

We have presented the results obtained in an experiment performed at Max Planck Institut für Quantenoptik in which we used the ASTERIX laser to investigate the possibilities of SXCM as a useful tool in biology. The high energy of the laser system and the high irradiances on the target allowed us to use several diagnostics to have a shot-to-shot characterisation of the X-ray source; moreover, it allowed us to irradiate up to 12 samples per shot, increasing the number of obtained images and improving the statistics.

We used different biological samples, in order to evaluate the capability of this technique to show details inside cells with different wall thicknesses, and to stress the limit of spatial resolution.

The number of photoresists which gave images was about 30% of the total; this percentage could be increased by having more reliable techniques of sample preparation. In fact, several of the photoresists could not be analysed because of damages to the surface of the PMMA made during the preparation or because the silicon nitride window broke in the vacuum chamber before exposure.

Our results indicate a good reproducibility of the image quality, and therefore suggest that the technique is reliable. This could be further improved with a better control on the amount of water layer present between the sample, the window and the photoresist.

The pictures of yeast cells, which are characterised by thick cell walls, show that even in this case it is possible to get information of the internal cell structure, while in the images of green algae one can observe a larger amount of internal details.

Details as thin as 50 nm can be neatly observed in pig sperm cells, demonstrating the capability of this technique to reach its theoretical limit.

The authors acknowledge the fruitful help of all the technical staff of the Max Planck Institut für Quantenoptik. A special thank must go to P. Anastasi, who provided the photo resists. This work has been supported by the European Union, under the Program "Human Capital and Mobility: Access to Large Scale Facilities" (contract n. ERB-CH-CT92-0006).

References

1. T.W. Ford *et al.*, Proc. SPIE **1741**, 351 (1992)
2. T.W. Ford, A.D. Stead, R.A. Cotton, Electron Microsc. Rev. **4**, 269 (1991)
3. J. Fletcher, R. Cotton, C. Webb, Proc. SPIE **1741**, 142 (1992)
4. A.D. Stead, A.M. Page, T.W. Ford, Proc. SPIE **2523**, 40 (1995)
5. H. Kondo, T. Tomie, J. Appl. Phys. **75**, 3798 (1994)
6. G.F. Foster *et al.*, Rev. Scient. Instr. **63**, 599 (1992)
7. A.D. Stead *et al.*, Proc. SPIE **1741**, 325 (1992)
8. R.A. Cotton *et al.*, Proc. SPIE **1741**, 204 (1992)
9. P. Albertano *et al.*, J. Microsc. **187**, 96 (1997)
10. I.C.E. Turcu *et al.*, Phys. Medica **10**, 93 (1994)
11. D. Batani *et al.*, Proc. SPIE **1503**, 479 (1991)
12. P. Celliers, K. Eidmann, Phys. Rev. A **41**, 3270 (1990)
13. K. Eidmann, T. Kishimoto, Appl. Phys. Lett. **49**, 377 (1986)
14. A.V. Vinogradov, V.N. Shlyaptsev, Sov. J. Quant. Electron. **17**, 1 (1987)
15. K. Eidmann, M. Kühne, P. Müller, G.D. Tsakiris, J. X-Ray Sci. Technol. **2**, 259 (1990)
16. G.D. Tsakiris, Proc. SPIE **1358**, 174 (1990)
17. P.A.F. Anastasi, R.E. Burge, Preparation and characterisation of silicon nitride membranes for SXCM, in *X-Ray Microscopy III* (Springer, 1992), pp. 341–343
18. D. Batani, A. Masini, E. Conte, A. Pozzi, C. Lora Lamia Donin, F. Cotelli, M. Moret, M. Costato, E. Turcu, N. Lisi, R. Allot, Phys. Medica **15**, 151 (1998)
19. A.D. Stead *et al.*, Proc. SPIE **2523**, 202 (1995)
20. L. Castellani Ceresa, R. Colombo, F. Cotelli, C. Lora Lamia Donin, Expl. Cell. Biol. **54**, 112 (1986)
21. C. Lora Lamia Donin *et al.*, J. Ultrastruc. Res. **96**, 12 (1986)
22. M.V. Klein, T.E. Furtak, *Optics* (Wiley, New York, 1986)
23. B.L. Henke, E.M. Gullikson, J.C. Davis, At. Data Nucl. Data Tab. **54**, 181 (1993)
24. D. Batani, C. Botto, F. Bortolotto, A. Masini, A. Bernardinello, M. Moret, M. Milani, K. Eidmann, G. Poletti, F. Cotelli, C. Lora Lamia Donin, S. Piccoli, A. Stead, T. Ford, A. Marranca, F. Flora, L. Palladino, L. Reale, Phys. Medica **16**, 49 (2000)